JVI Journals.ASM.org

The H275Y Neuraminidase Mutation of the Pandemic A/H1N1 Influenza Virus Lengthens the Eclipse Phase and Reduces Viral Output of Infected Cells, Potentially Compromising Fitness in Ferrets

Lady Tatiana Pinilla,[a] Benjamin P. Holder,[b] Yacine Abed,[a] Guy Boivin,[a] and Catherine A. A. Beauchemin[b]

Infectious Disease Research Centre, CHUQ-CHUL and Laval University, Québec City, Québec, Canada,[a] and Department of Physics, Ryerson University, Toronto, Ontario, Canada[b]

The H275Y amino acid substitution of the neuraminidase gene is the most common mutation conferring oseltamivir resistance in the N1 subtype of the influenza virus. Using a mathematical model to analyze a set of *in vitro* experiments that allow for the full characterization of the viral replication cycle, we show that the primary effects of the H275Y substitution on the pandemic H1N1 (H1N1pdm09) strain are to lengthen the mean eclipse phase of infected cells (from 6.6 to 9.1 h) and decrease (by 7-fold) the viral burst size, i.e., the total number of virions produced per cell. We also find, however, that the infectious-unit-to-particle ratio of the H275Y mutant strain is 12-fold higher than that of the oseltamivir-susceptible strain (0.19 versus 0.016 per RNA copy). A parallel analysis of the H275Y mutation in the prior seasonal A/Brisbane/59/2007 background shows similar changes in the infection kinetic parameters, but in this background, the H275Y mutation also allows the mutant to infect cells five times more rapidly. Competitive mixed-strain infections *in vitro*, where the susceptible and resistant H1N1pdm09 strains must compete for cells, are characterized by higher viral production by the susceptible strain but suggest equivalent fractions of infected cells in the culture. In ferrets, however, the mutant strain appears to suffer a delay in its infection of the respiratory tract that allows the susceptible strain to dominate mixed-strain infections.

In 2009, the World Health Organization (WHO) declared the first influenza pandemic of this century and described the virus (H1N1pdm09) as naturally resistant to adamantanes but susceptible to the neuraminidase (NA) inhibitors oseltamivir and zanamivir (10, 29). In the past 3 years, isolated cases of oseltamivir resistance in H1N1pdm09 strains have been reported—almost always associated with the H275Y mutation within the NA gene—but the overall level of resistance has remained relatively low (42) at ~1% in the United States (47), <1% in Canada (40), ~2.5% in Europe (14, 26), and <1.6% worldwide (26). In the United States, the fraction of cases of resistance not associated with oseltamivir exposure increased significantly from 11% in the 2009-2010 season to 75% in the 2010-2011 season (47). A few small clusters of oseltamivir resistance cases not associated with treatment and likely involving transmission of H1N1pdm09 mutant (MUT) strains have been reported in Europe (20, 32), Australia (25, 27), and Vietnam (34). The pandemic strain completely displaced the prior seasonal H1N1 strain (A/Brisbane/59/2007), which, in the 2008-2009 season, was nearly 100% resistant to oseltamivir (11, 18). That dominance of an oseltamivir-resistant H275Y MUT strain was surprising at the time because it had been shown that the mutation usually compromised strain fitness (30). A return to widespread oseltamivir resistance, with a mutated H1N1pdm09 virus, could have significant public health consequences (19).

Laboratory experiments have often been used to assess a particular influenza virus strain's phenotype in cell culture and animal models, particularly in relation to oseltamivir resistance. Prior to 2007, experiments demonstrated strongly attenuated growth of H275Y MUT strains of H1N1 *in vitro* (1, 21), a higher viral titer inoculum required for the infection of ferrets (21, 30), and generally less-pathogenic infections in ferrets, quantified by reduced fevers and smaller inflammatory cell counts in nasal washes (30). This mirrored the seasonal epidemic situation at the time, in which oseltamivir resistance emerged almost exclusively under drug pressure and in immunocompromised patients (3). Thus, the subsequent dominance of the A/Brisbane/59/2007 (H1N1) H275Y MUT strain in 2007-2008 and 2008-2009 came as a surprise. Since its emergence, however, the strain has been found to have a replication capacity *in vitro* equivalent to or greater than that of its susceptible counterpart (5) and to produce comparable infections in ferrets (28, 35). Experiments with small numbers of animals ($n \leq 5$) have been unable to demonstrate a difference in transmission efficiency between the susceptible and resistant strains (2, 28). A recent experiment with a larger population of guinea pigs ($n \cong 20$) did show a significantly more rapid transmission of the resistant strain but did not find significant enhancement of the transmission frequency (8). Studies *in vitro* determined that the fitness of the A/Brisbane/59/2007 MUT strain was likely associated with its prior acquisition (between 1999 and 2006) of permissive mutations of the NA gene, which increased both the activity and the surface expression of NA (6). The reversion of one such permissive mutation, R222Q, in A/Brisbane/59/2007 NA was found to reduce viral production in infected ferrets (2).

Laboratory characterization of the effect of the H275Y mutation in the H1N1pdm09 background has yielded mixed conclusions. Unlike the growth of pre-2007 seasonal H1N1 strains, that

Received 2 January 2012 **Accepted** 12 July 2012

Published ahead of print 15 July 2012

Address correspondence to Catherine A. A. Beauchemin, cbeau@ryerson.ca, or Guy Boivin, Guy.Boivin@crchul.ulaval.ca.

L.T.P. and B.P.H. contributed equally to this study.

Supplemental material for this article may be found at http://jvi.asm.org/.

doi:10.1128/JVI.07244-11

of the H1N1pdm09 H275Y MUT (H1N1pdm09-MUT) strain is not severely compromised *in vitro* or in ferrets (9, 12, 15, 31). Contact transmissions of H1N1pdm09-MUT between ferrets have been successful in all of the experiments reported (15, 16, 35, 38, 45). The results concerning airborne transmission, however, have been mixed, with some studies finding comparable (45, 46) or nonsignificant differences (12) in efficiency and others finding that H1N1pdm09-MUT was transmitted less efficiently (16) ($P = 0.04$, two-tailed Mantel-Cox test; M. É. Hamelin, personal communication) or suffered a delay with respect to the susceptible strain (31). Concise reviews of this prior work can be found elsewhere (7, 26, 42). Thus, current laboratory experiments provide little consistent evidence regarding factors that might influence the circulation of H1N1pdm09-MUT.

In this report, we make two contributions to the understanding of the fitness of H1N1pdm09 strains. First, we introduce a method to fully quantify the basic components of the viral replication cycle (e.g., the length of the eclipse phase and viral infectivity) *in vitro*. By considering a set of complementary experiments which highlight different aspects of viral replication, we were able to extract values for each quantitative measure with narrow confidence intervals (CIs) by using a mathematical model. This new quantitative characterization replaces generic, experiment-specific, descriptions of strain replication (e.g., attenuated growth, reduced fitness *in vitro*) with meaningful fundamental quantities representing the interaction of the virus with cells. We apply this method to translate subtle differences in the observed *in vitro* virus dynamics of H1N1pdm09-WT and H1N1pdm09-MUT into reliable quantitative estimates of the differences in replication induced by the H275Y mutation in the 2009 strain genetic background. We also characterize the effect of this mutation in the A/Brisbane/59/2007 (H1N1) strain background and perform a comparative analysis.

Second, we assessed the relative replication capacities of the two H1N1pdm09 strains by performing competitive mixed-infection experiments *in vitro* and in ferrets. While an infection with a pure inoculum demonstrates how each strain fares individually in separate hosts, a competitive infection with a mixed inoculum reveals which of the two strains would overtake the other when infecting the same host while competing for a shared pool of susceptible cells. Our model correctly predicts the dynamics of H1N1pdm09 mixed infections *in vitro*, without any additional assumptions or parameters, verifying the effectiveness of our method in characterizing each strain and predicting the outcome of their interactions. *In vitro*, in mixed infections with a 50:50 inoculation ratio, each strain infects the same number of cells, suggesting that they have equivalent fitness, whereas mixed infections of ferrets suggest a potential replicative advantage for the susceptible strain.

MATERIALS AND METHODS

Ethics statement. All procedures were approved by the Institutional Animal Care Committee at Laval University according to the guidelines of the Canadian Council on Animal Care (permit 2011055-1).

Viruses. The wild-type (WT) pandemic H1N1 influenza virus strain (H1N1pdm09-WT) used for all experiments—except those performed for confirmation of the analysis—was the first to be isolated in Québec City, Canada (A/Québec/144147/09; GenBank accession numbers FN434457 to FN434464); its NA H275Y MUT (H1N1pdm09-MUT) differs from the WT by only a single nucleotide in the NA gene. Recombinant H1N1pdm09-WT and H1N1pdm09-MUT viruses were rescued by reverse genetics as described previously (39). The natural isolates of H1N1pdm09 used to confirm the analysis of the recombinant strains were recovered from a boy (niWT, A/Québec/147023/09; GenBank accession numbers FN434440 to FN434447) and his father (niMUT, A/Québec/147365/09; GenBank accession numbers FN434448 to FN434456) who had been placed on oseltamivir prophylaxis and have been described previously (4). The A/Brisbane/59/2007-like WT and MUT H1N1 virus strains are also each natural isolates (A/Québec/15230/08 and A/Québec/15349/08, respectively) described previously (24).

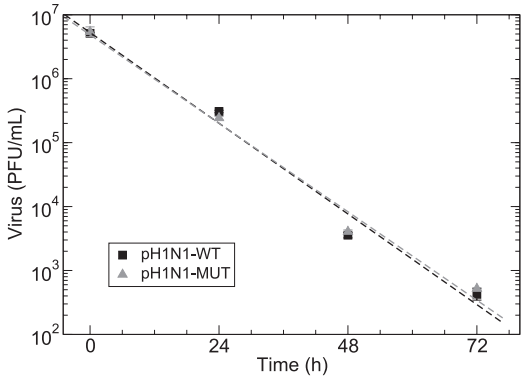

FIG 1 Mock-infection experiment to determine viral infectivity loss rate. H1N1pdm09-WT (squares, black) and H1N1pdm09-MUT (triangles, gray) viruses subjected to the physical conditions of the *in vitro* experiments (37°C, 5% CO_2) lose infectivity exponentially at the same rate, $c_{WT} = c_{MUT} = 0.13$ h^{-1}, corresponding to a virion infectious half-life of 5.3 h.

The exponential rate of viral infectivity loss, c, was determined for each H1N1pdm09 strain by a mock-infection assay (Fig. 1). Known titers of the H1N1pdm09-WT and H1N1pdm09-MUT viruses were incubated in separate wells with maintenance medium (but without cells) at 37°C in 5% CO_2; experiments (performed in triplicate) were terminated at 24, 48, and 72 h to determine the remaining infectious titers. The fitted decay rates were found to be identical for the two strains, $c = 0.13$ h^{-1} (95% CI, 0.11 to 0.15), corresponding to a virion infectivity half-life of 5.2 h.

***In vitro* replication experiments.** For both multiple-cycle (MC) and single-cycle (SC) viral yield experiments, ST6GalI-transfected Madin-Darby canine kidney (MDCKα2,6) cells, which overexpress α-2,6 sialic acid receptors, were used (17). For the SC experiment, confluent cells in 12-well plates were infected with an inoculum of 4×10^6 PFU, representing a multiplicity of infection (MOI) of 4. Supernatants were harvested every hour for the first 10 h and then every 2 to 3 h until 18 h postinfection. For the MC experiment, cells were infected with 50 PFU (MOI = 5×10^{-5}) of pure H1N1pdm09-WT or H1N1pdm09-MUT recombinants (39) or one of three WT-MUT mixtures, 80:20, 20:80, or 50:50. Supernatants were collected every 12 h until 72 h postinfection in three independent experiments with three replicates each. Additional measurements at different time points were made in triplicate in the pure-population MC experiments. Supernatants were stored at −80°C until their use for RNA isolations, real-time RT-PCR, and/or viral titration by standard plaque assay on MDCKα2,6 cells.

RNA extraction. Total RNA was isolated from 200 μl of each thawed specimen or culture using the robotic MagNA Pure instrument and the MagNA Pure LC total nucleic acid isolation kit (Roche Applied Science, Mannheim, Germany) according to the manufacturer's instructions, with a total elution volume of 50 μl. Isolated RNA was stored at −80°C.

NA gene H275Y discriminatory real-time RT-PCR assay. To discriminate between WT and oseltamivir-resistant strains of H1N1pdm09, a modified version of a real-time reverse transcription (RT)-PCR method reported by van der Vries et al. (48) was used. This technique requires reverse (panN1-H275-sense 5′-CAGTCGAAATGAATGCCCCTAA-3′) and forward (panN1-H275-antisense 5′-TGCACACACATGTGATTTCACTAG-

3′) primers for both the WT and H275Y MUT viruses and two labeled, allele-specific probes, panN1-275H-probe (5′-TTATCACTATGAGGAATGA–6-carboxyfluorescein [FAM]/BHQ-1) and panN1-275Y-probe (5′-TTATTACTATGAGGAATGA–HEX/BHQ-1, where underlining indicates locked nucleic acids). The discrimination properties of specific probes are due to locked nucleic acids which contain the single nucleotide polymorphism of interest at the 5′ end and increase melting temperatures, thus allowing the probe to be shorter with increased discriminatory capacities. The limit of detection is 50 copies for the MUT (H275Y) target and 10 to 50 copies for the WT target.

The one-step RT-PCR mixture was prepared in a 25-μl reaction volume containing 6.25 μl of TaqMan Fast Virus 1-Step Master Mix (Applied Biosystems, Foster City, CA), 0.8 μl of both the reverse and the forward primers, 1.0 μl of each probe, and 4.0 μl of RNA extract. The amplification process was performed in a LightCycler 480 real-time thermocycler (Roche) under the following cycling conditions: 60°C for 30 min (RT) and 95°C for 5 min (DNA polymerase activation), followed by 45 cycles of 95°C for 20 s (denaturation) and 62°C for 1 min (annealing). One reaction was performed for each sample with the WT and the H275Y probes and the common reverse and forward primers. Data acquisition was performed with both FAM and HEX filters during the annealing/extension step.

Ferret experiments. Four groups of four seronegative male ferrets (12 to 18 weeks old, 900 to 1,500 g) (Triple F Farms, Sayre, PA) housed in individual cages were anesthetized with isoflurane and received, by intranasal instillation, 250 μl (125 μl/nare) of phosphate-buffered saline (PBS) containing 10^5 PFU of H1N1pdm09-WT or H1N1pdm09-MUT as a pure population or a mixture of the two (WT/MUT ratio, 20:80 or 50:50). Ferrets were weighed and their temperatures were measured (by rectal thermometer) every day until 14 days postinfection (dpi). Ferrets were also observed for possible signs of infection such as sneezing, reduced activity, and reduced interest in food. However, a particular scoring system—such as that developed by Reuman et al. (43) for measuring the nasal discharge and the activity level of ferrets—was not used. Nasal wash samples were collected every 12 h until 72 h postinfection and subsequently on a daily basis until 7 dpi by instillation of 5 ml of PBS into the external nares of the animals. Samples were stored at −80°C until use for RNA isolation and real-time RT-PCR or for viral titration by standard plaque assay with MDCKα2,6 cells. Serum samples were collected from each ferret before intranasal infection and on day 14 to evaluate levels of specific antibody against H1N1pdm09 by using standard hemagglutination inhibition (HI) assays. The animal procedures were conducted at biocontainment level 2+ in accordance with the animal experimentation guidelines of the Centre Hospitalier Universitaire de Québec.

Mathematical model. Viral yield experiments (SC and MC) were simulated by using the following multicompartment ordinary differential equation (ODE) model:

$$\dot{T} = -\beta T V_{\mathrm{PFU}}$$

$$\dot{E}_1 = \beta T V_{\mathrm{PFU}} - \frac{n_E}{\tau_E} E_1$$

$$\dot{E}_j = \frac{n_E}{\tau_E} E_{j-1} - \frac{n_E}{\tau_E} E_j \text{ for } j = (2, \ldots, n_E)$$

$$\dot{I}_1 = \frac{n_E}{\tau_E} E_{n_E} - \frac{n_I}{\tau_I} I_1$$

$$\dot{I}_j = \frac{n_I}{\tau_I} I_{j-1} - \frac{n_I}{\tau_I} I_j \text{ for } j = (2, \ldots, n_I)$$

$$\dot{V}_{\mathrm{PFU}} = \rho p \sum_{j=1}^{n_I} \frac{I_j}{N} - (c + c_R) V_{\mathrm{PFU}}$$

$$\dot{V}_{\mathrm{RNA}} = p \sum_{j=1}^{n_I} \frac{I_j}{N} - c_R V_{\mathrm{RNA}}$$

which describes the infection of a population of N susceptible target cells (T) at a rate (βV_{PFU}) proportional to the concentration of infectious virions (V_{PFU}). Newly infected cells first undergo an eclipse phase (E) of average duration τ_E before becoming infectious (I) and producing virus at a constant rate p for an average time τ_I. The two variables V_{PFU} and V_{RNA} represent the infectious (number of PFU/ml/h) and total (number of RNA copies/ml) virus concentrations, whose kinetics are controlled by the virus production rate (p in number of RNA copies/m/h), the conversion factor between virus produced and virus observed by titration (ρ in number of PFU/RNA copy), the rate at which infectious virus lose infectivity (c), and a rate of virus particle loss (c_R). The quoted production rate per cell, p_{RNA}, is equal to p times the supernatant volume (0.5 ml) divided by the number of cells in the culture (10^6).

In previous work, we have shown that the assumption that cells spend an exponentially distributed amount of time in the eclipse or infectious phase—implicit to the simpler, $n_I = n_E = 1$, ODE models—is unrealistic (22, 23). This is because exponentially distributed durations for these phases imply that cells can immediately begin viral production upon infection, can cease viral production immediately after it is initiated, and can produce virus indefinitely. To impose more biologically realistic conditions on the time spent by a cell in the infected phases, we subdivided each phase using n_E (or n_I) equations, such that these times are gamma distributed with a mean of τ_E (or τ_I) and a standard deviation of $\sigma_E = \tau_E/\sqrt{n_E}$ or ($\sigma_I = \tau_I/\sqrt{n_I}$).

When simulating competitive mixed-infection experiments, the infection of target cells was determined by

$$\dot{T} = -\beta^{WT} T V_{\mathrm{PFU}}^{WT} - \beta^{MUT} T V_{\mathrm{PFU}}^{MUT}$$

where $V_{\mathrm{PFU}}^{\mathrm{WT}}$ and $V_{\mathrm{PFU}}^{\mathrm{MUT}}$ are the concentrations of the WT and H275Y MUT strains, respectively, and a different rate constant, β, was assumed for infection by each strain. By prohibiting the coinfection of cells, two parallel instances of the remaining equations in the ODE model described above, one for each strain, were used to completely describe the dynamics.

To determine the *in vitro* infectivity of a particular strain, we used the infecting time, $t_{\mathrm{infect}} = \sqrt{2/(\rho p \beta)}$, which is the amount of time required for a single infectious cell to cause the latent infection of one more, within a completely susceptible population (24). Strains with a shorter infecting time have a higher infectivity. The basic reproductive number, R_0, defined as the number of cells secondarily infected by a single infectious cell in a completely susceptible population, was calculated numerically for each set of extracted parameter values. Best-fit values and the statistics of derived quantities—including the RNA viral burst size, $b = p_{\mathrm{RNA}} \times \tau_I$, and the number of infectious units per particle, R_0/b—were calculated by using the other extracted parameter values for each fit.

A number of parameter values were fixed in all simulations. The rate at which infectious H1N1pdm09-WT and H1N1pdm09-MUT virions lose infectivity was determined independently in mock-infection experiments (described above) and was fixed at a value of $c = 0.13\ \mathrm{h}^{-1}$. Sensitivity analysis of the model (not shown) showed that the standard deviation of the infectious life span was not identifiable. We therefore fixed $n_I = 100$ ($\sigma_I = 4$ h when $\tau_I = 40$ h). A constant delay of virus production for cells infected in the simulated inoculation period (1 h prior to $t = 0$) was required for the simulation of MC experiments; this was fixed at 12.3 h for both strains. Finally, the rate of infectious virus production in simulations of the SC experiment was allowed to differ from that of the MC experiment and was effectively fixed by the normalization of the SC experimental data to unity. This normalization was necessary to avoid the confounding effects of defective interfering particles, which can cause highly variable virus levels in high-MOI infections (24, 36).

Regression and statistics. Nonlinear least-squares regression of the model to the SC and MC viral yield data sets simultaneously was performed by using the Octave 3.2.4 (www.octave.org) implementation of the Levenberg-Marquardt algorithm, leasqr. In this analysis, parameter values were assumed to be the same for the two experiments but initial conditions were adjusted to reflect the experimental preparations; the 1-h

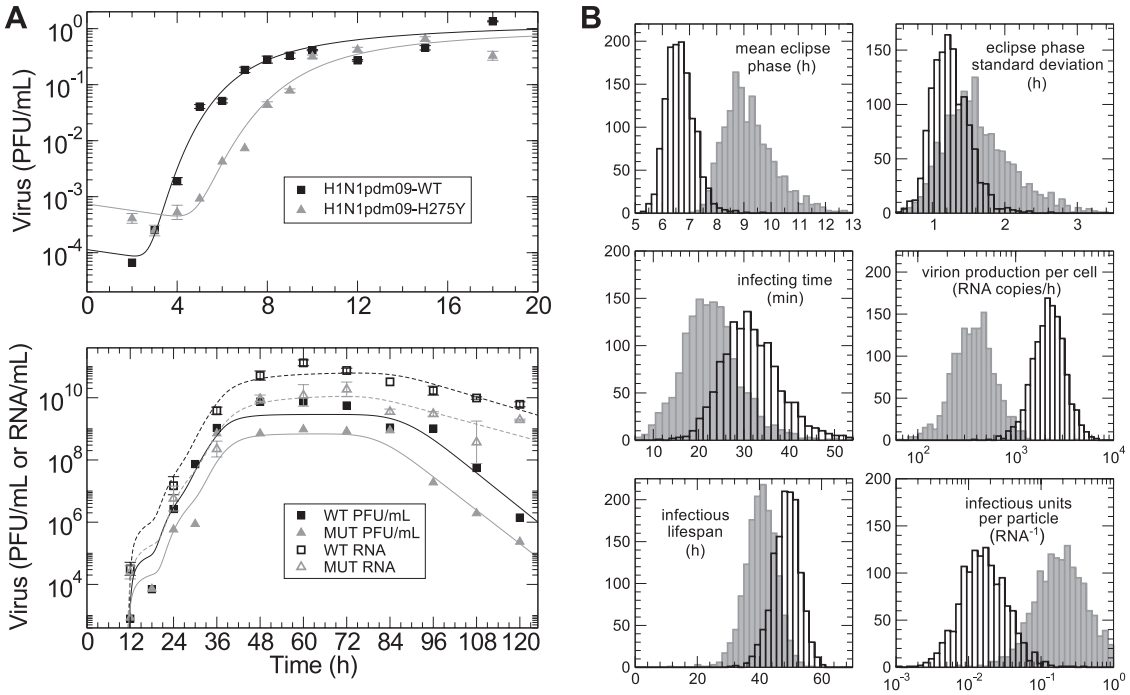

FIG 2 SC and MC viral yield experiments. (A) Experimental values of infectious virus (PFU/ml, filled symbols) and total viral load (RNA/ml, open symbols) for the H1N1pdm09-WT (squares, black) and H1N1pdm09-MUT (triangles, gray) strains in SC (top) and MC (bottom) viral yield experiments. Best-fit model virus curves are overplotted as lines (infectious, solid; total, dashed). (B) Histograms of parameter values determined from fits to 1,000 bootstrap replicates of the SC and MC data for the H1N1pdm09-WT (black) and H1N1pdm09-MUT (gray) strains.

experimental infection of cells (which produced an MOI of 4 for the SC and $50/10^6$ for the MC) was numerically simulated such that the desired MOI and a small residual amount of virus were present at $t = 0$. Fit residuals were sampled with replacement (within each experiment type) to produce 1,000 bootstrap replicates of the data sets (13), from which 95% CIs were determined for the extracted parameter values. The significance level (P value) for the difference in estimated parameter values between the two (WT and MUT) strains was determined by a two-sided Z test, with variance values taken from the bootstrap-derived parameter values. Specifically, for a particular parameter Θ (e.g., the mean eclipse phase, τ_E), the test statistic $TS = \frac{\Theta^{WT} - \Theta^{MUT}}{\sqrt{\sigma^2_{WT} + \sigma^2_{MUT}}}$, with the variance values σ^2_{WT} and σ^2_{MUT} calculated directly from the bootstrap-derived values for the WT and MUT strains, was assumed to have the standard normal form. When the distributions of bootstrap values for each strain were better described as lognormal (i.e., for the mean eclipse phase, the production rate per cell, the viral burst size, the basic reproductive number, and the number of infectious units per particle), the above analysis was performed on the log of the parameter instead.

RESULTS

Quantification of the H1N1pdm09 replication cycle *in vitro*. The method we introduce here enables the independent quantification of each of the fundamental phases of viral replication within a cell, i.e., infection, a period of eclipse (latent infection), virus production, and virus-induced cell death. This is achieved by analyzing parallel SC and MC viral yield experiments performed for each H1N1pdm09 strain (H1N1pdm09-WT or H1N1pdm09-MUT) under the same experimental conditions (see Materials and Methods). The SC experiment, in which the cell culture is infected with a large inoculum (MOI = 1), allows the characterization of the eclipse phase due to the synchronized infection of nearly all of the cells (22). The MC experiment, in which the cell culture is infected with a much smaller inoculum (MOI $\ll$ 1), provides a complementary picture, highlighting the progressive consumption of susceptible cells through an exponential increase of the virus. We fitted the ODE model (described above) to the SC and MC data sets simultaneously (Fig. 2A) and determined values for the relevant viral kinetic parameters for each H1N1pdm09 strain (Table 1 and Fig. 2B).

The H275Y amino acid substitution caused a significant change in a number of quantitative measures of the infection cycle. The mean eclipse phase for H1N1pdm09-MUT was significantly longer (9.1 h versus 6.6 h for H1N1pdm09-WT; $P = 0.013$), and the viral production rate per MDCKα2,6 cell was significantly reduced (from 2,200 to 370 RNA copies/h; $P = 0.004$). The difference in the eclipse phase can be seen directly in the SC data, as a longer delay of H1N1pdm09-MUT viral titer growth. The ratio of the production rates can also be approximately determined directly from the data by taking the ratio of the peak RNA virus levels in the MC experiment (this follows by setting $\dot{V}_{RNA}$ equal to 0 in the ODE model, assuming that the WT and MUT values of c_R are approximately equal—their fitted values were 0.07 and 0.08 h^{-1}, respectively—and assuming that all cells are infectious at the time of viral peak). In the MC experiment (Fig. 2A, bottom), this ratio was ~6, matching the ratio of viral production rates determined above. The higher viral production rate of H1N1pdm09-WT is an important fact to consider when analyzing the competitive mixed-infection results presented below.

The average infectious life span of an MDCKα2,6 cell (the amount of time for which it produces virus) approximately determines the width of the MC viral titer (PFU) curve and the length of

TABLE 1 Best-fit viral kinetic parameters for WT and MUT H1N1pdm09[a]

Parameter	Value (95% CI)		*P* value[b]
	WT	MUT	
Mean eclipse period, τ_E (h)	6.6 (5.8–7.7)	9.1 (7.8–11.6)	0.013
Eclipse period SD, σ_E (h)	1.2 (0.81–1.8)	1.6 (0.88–2.8)	0.49
Infecting time, t_{infect} (min)	31 (20–47)	22 (11–38)	0.35
MDCKα2,6 infectious life span, τ_I (h)	49 (39–57)	41 (30–50)	0.24
Virion infectious half-life, ln2/c (h)	5.2	5.2	
Production rate/cell, p_{RNA} (no. of RNA copies/h)	2,200 (960–4,600)	370 (130–960)	0.004
Viral burst size, $b = p_{RNA} \times \tau_I$ (no. of RNA copies)	110 (47–220) $\times 10^3$	15 (5.3–37) $\times 10^3$	0.001
Basic reproductive no., R_0	1.7 (0.66–4.3) $\times 10^3$	3.0 (0.82–12) $\times 10^3$	0.51
No. of infectious units per particle, R_0/b	16 (3.8–68) $\times 10^{-3}$	190 (36–1,000) $\times 10^{-3}$	0.031

[a] Fitted parameter values for WT and MUT H1N1pdm09 with 95% CIs from bootstrap replicates of SC and MC viral yield experiments.
[b] WT versus MUT.

its plateau (seen in the PFU data between 42 and 72 h) where virus production is balanced by the loss of virion infectivity. We determined infectious cell life spans of 49 h for H1N1pdm09-WT and 41 h for H1N1pdm09-MUT ($P = 0.24$). Additionally, by multiplying the infectious life span by the viral production rate per cell, we can obtain the viral burst size for each strain, i.e., the total number of virions produced by an infected cell. The burst size was found to be significantly larger for H1N1pdm09-WT (1.1×10^5 versus 1.5×10^4 RNA copies; $P = 0.001$).

We quantified the infectivity of a virus strain by its infecting time, which is defined as the amount of time required for a single infectious cell to cause the infection of one more cell in a completely susceptible population (see Materials and Methods). This measure therefore depends on both the rate at which virions are produced by cells and the relative infectivity of these virions. The estimated infecting times were 31 min for H1N1pdm09-WT and 22 min for H1N1pdm09-MUT ($P = 0.35$). To estimate the proportion of infectious virions produced by each strain, we numerically calculated the basic reproductive number, which is defined as the number of secondary infections caused by a single infectious cell. By this definition, the number of infectious units per RNA particle is therefore equal to the basic reproductive number divided by the viral burst size. Like the infecting time, the basic reproductive number was not significantly different for the two strains. We found, however, that the infectious-unit-to-particle ratio was 12 times higher ($P = 0.031$) for H1N1pdm09-MUT. Thus, while H1N1pdm09-WT-infected cells produce a larger number of virions than H1N1pdm09-MUT-infected cells, the higher infectivity of H1N1pdm09-MUT virions compensates for this discrepancy such that infectious virions are produced by cells at equivalent rates (34 h^{-1} for the WT versus 72 h^{-1} for the MUT; $P = 0.33$).

To verify that our findings generalize to other H1N1pdm09 backgrounds, we reproduced the SC and MC viral yield experiments with a WT-MUT strain pair of H1N1pdm09 natural isolates (Fig. 3). A good fit to the data from the pair of natural isolates (niWT and niMUT) was obtained by using the key parameter values determined for the recombinant pair. This serves as both a qualitative and a quantitative confirmation of the effect of the H275Y mutation on the replication kinetics of H1N1pdm09, presented above.

Comparative analysis of seasonal strain A/Brisbane/59/2007. Having determined the effect of the H275Y mutation on the infection kinetic parameters of H1N1pdm09, we performed the same (SC and MC) analysis with A/Brisbane/59/2007-like strains (both WT and H275Y MUT) from the 2008-2009 influenza season. These data were presented previously (24), though without this full analysis, and are not reproduced here (see the supplemental material). The results of this new SC and MC fitting analysis of WT and MUT A/Brisbane/59/2007 are given in Table 2. A comparison of the results to those obtained with H1N1pdm09 are presented in Fig. 4.

It is clear that the H275Y mutation has a similar effect in the A/Brisbane/59/2007 strain background. In particular, the mean eclipse phase is significantly longer for the MUT strain ($P < 0.001$). One notable distinction, however, is that there is a signif-

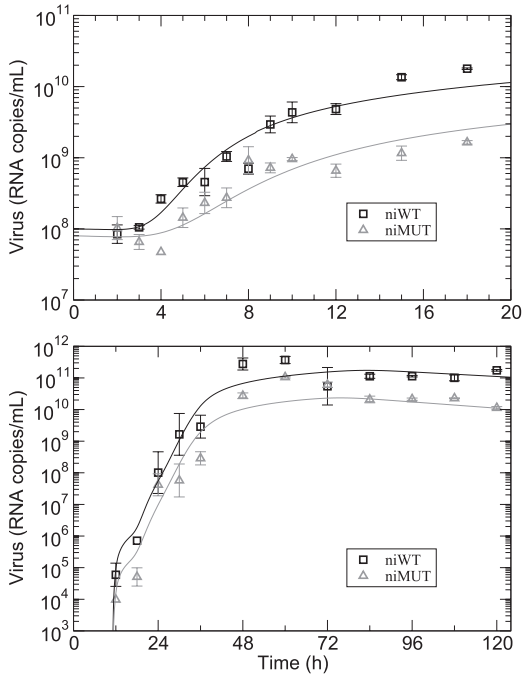

FIG 3 SC and MC viral yield experiments for a second pair of H1N1pdm09 strains, i.e., natural isolates A/Québec/147023/09 (niWT) and A/Québec/147365/09 (niMUT). Total viral loads were determined by RT-PCR (niWT, black squares; niMUT, gray triangles) in the SC (top) and MC (bottom) experiments. Best-fit model curves, assuming that all parameters except σ_E and c_R remained fixed to the values found for the original strains (Fig. 2 and Table 1), are overplotted. The fitted values for the niWT and niMUT strains are $\sigma_E =$ 1.8 and 3.3 h and $c_R = 0.014$ and 0.019 h^{-1}, respectively.

TABLE 2 Best-fit viral kinetic parameters for WT and MUT A/Brisbane/59/2007[a]

Parameter	Value (95% CI)		
	WT	MUT	*P* value[b]
Mean eclipse period, τ_E (h)	6.1 (6.0–6.7)	8.0 (7.4–9.1)	<0.001
Eclipse period SD, σ_E (h)	0.47 (0.46–0.92)	1.2 (0.83–1.9)	0.014
Infecting time, t_{infect} (min)	18 (13–21)	3.4 (2.0–5.1)	<0.001
MDCKα2,6 infectious life span, τ_I (h)	14 (11–18)	16 (10–23)	0.57
Virion infectious half-life, ln2/c (h)	3.7 (3.4–4.0)	3.5 (3.1–3.9)	0.43
Basic reproductive no., R_0	1.7 (1.1–3.3) × 10^3	48 (17–158) × 10^3	<0.001

[a] Fitted parameter values for WT and MUT A/Brisbane/59/2007 with 95% CIs from bootstrap replicates of SC and MC viral yield experiments. For the data and fitted model curves, see the supplemental material.
[b] WT versus MUT.

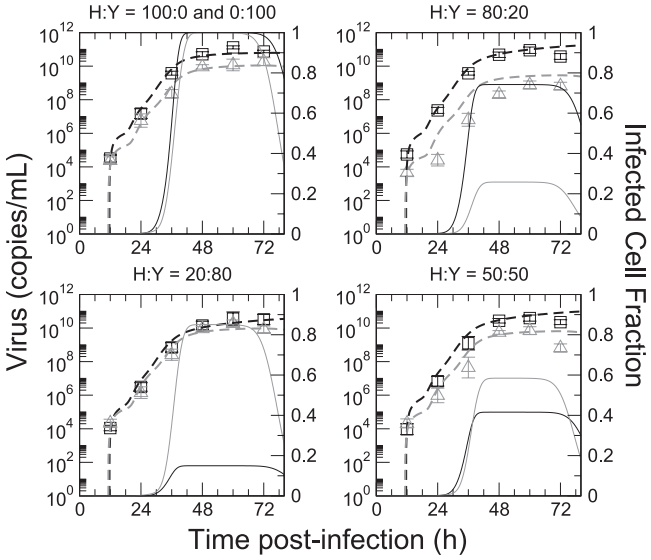

FIG 5 Competitive mixed-infection experiments with H1N1pdm09-WT and H1N1pdm09-MUT *in vitro*. Experimental values of H1N1pdm09-WT (squares, black) and H1N1pdm09-MUT (triangles, gray) are given for different initial infection ratios (H:Y, WT/MUT ratio). Model-predicted virus curves (dashed lines) for H1N1pdm09-WT (black) and H1N1pdm09-MUT (gray) and the fraction of cells infected by each strain (solid lines) are plotted, using only the parameter values determined from fits to the pure-population SC and MC experiments.

icant difference between the infecting times of WT and MUT A/Brisbane/59/2007 ($P < 0.001$)—with the MUT possessing a shorter infecting time and thus higher infectivity—while there was not a significant difference for the H1N1pdm09 strains. Moreover, the infecting times of both A/Brisbane/59/2007 strains are significantly shorter than those of H1N1pdm09-WT ($P < 0.05$). The higher infectivity of the A/Brisbane/59/2007 MUT strain is also evidenced by its basic reproductive number, which is >10-fold larger than that of all other strains ($P < 0.001$). The A/Brisbane/59/2007 strains also have significantly shorter infectious life spans than the H1N1pdm09 strains ($P < 0.05$). This corroborates our own experimental observations that dead-cell plaques are observed only at very late times in H1N1pdm09, compared to A/Brisbane/59/2007, titration experiments, although foci of infected cells are observed early on (data not shown).

Competitive mixed-infection experiments *in vitro*. To observe the effects of strain-specific parameter differences in direct competition, we performed competitive mixed-infection experiments with the two H1N1pdm09 strains *in vitro*. MDCKα2,6 cells were infected with a mixture of the virus strains at three WT/MUT ratios, 80:20, 20:80, and 50:50, adding up to a total inoculum of 50 PFU (MOI = $50/10^6 = 5 \times 10^{-5}$). The mathematical model was adjusted to allow for two virus strains, under the assumption of no coinfection of cells; a cell can be infected by either the WT or the MUT strain, but once infected by one strain, it is no longer available for infection by the other strain. This allowed us to simulate the mixed-infection experiments by using the previously extracted parameter values for each strain without any additional assumptions or parameters. The results of these experiments, along with the virus and infected-cell values predicted by the model, are shown in Fig. 5. Generally, the model predictions matched the experimental values very well. This success of the model at predicting the results of an independent set of experiments lends weight to the validity of the extracted values of the infection kinetic parameters for each strain.

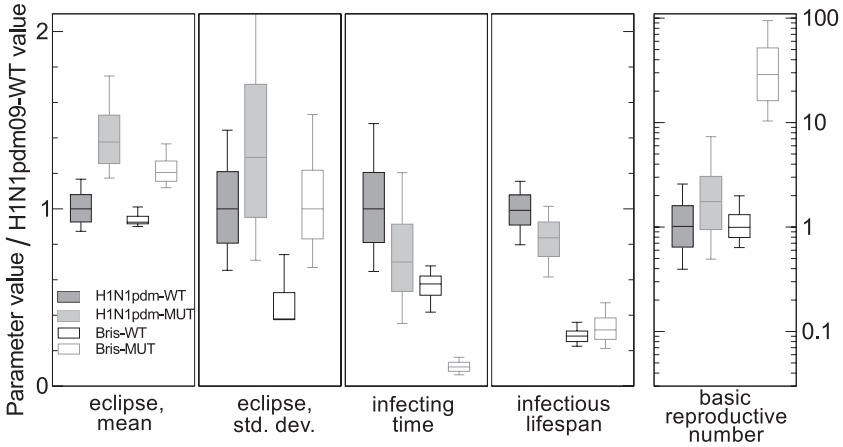

FIG 4 Comparison of H1N1pdm09 and A/Brisbane/59/2007 viral kinetic parameter values. Parameter values of the four strains, normalized to the value of H1N1pdm09-WT, are shown. Vertical boxes and bars represent the 68 and 95% CIs, respectively, determined from the bootstrap replicates to SC and MC data. Note that the comparison for the basic reproductive number is logarithmic.

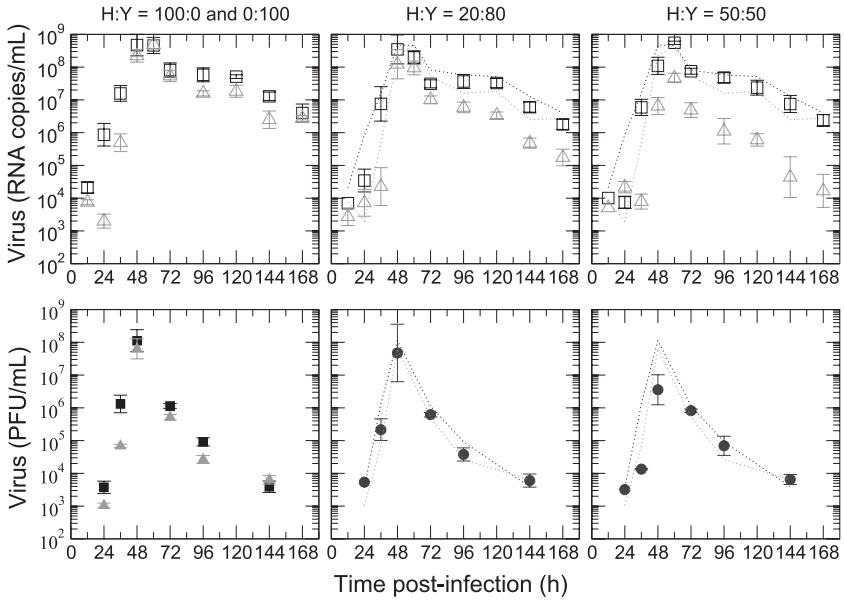

FIG 6 Pure and competitive-mixture infections of ferrets with H1N1pdm09-WT and H1N1pdm09-MUT. Total virus counts (top row) of the H1N1pdm09-WT (squares, black) and H1N1pdm09-MUT (triangles, gray) strains over time in infected ferrets and corresponding infectious-titer measurements (bottom row) are shown. The leftmost panel in each row shows the results of infections with purely H1N1pdm09-WT and purely H1N1pdm09-MUT (the two data sets are overplotted for comparison), while the other two panels show mixed infections at different initial infection ratios (H:Y, WT/MUT ratio). Each point is the geometric average of four ferrets, and geometric standard errors are indicated. The dotted lines in the right two panels indicate the values of the pure-population viral load from the leftmost panel for reference.

In terms of total virus produced, the H1N1pdm09-WT strain shows a clear dominance in the mixed-infection results. At the 50:50 infection ratio, for example, the H1N1pdm09-WT virus counts are significantly larger than the H1N1pdm09-MUT values for all but the first two time points ($P < 0.05$; rank-sum test). The model prediction for the infected-cell fractions, however, suggests that the H1N1pdm09-MUT strain infected a larger fraction of the available cells. Taking into account the 95% CI found above for each parameter, this difference in the fractions of cells infected by the two strains is not significant, i.e., at the 50:50 infection ratio, the model predicts that each strain infects approximately half of the cells. This is consistent with our previously extracted parameters; if the H1N1pdm09-WT strain infects the same number of cells as the H1N1pdm09-MUT strain, it will produced a larger proportion of the total virus because of its ~6-fold higher viral production rate. The infection of an equal fraction of the cell culture would also be consistent with the similar basic reproductive numbers determined for the two strains.

Pure and competitive infections of ferrets. To directly compare the replication capacities of the H1N1pdm09 viruses *in vivo*, four groups of four ferrets were infected with 10^5 PFU of pure strain H1N1pdm09-WT or H1N1pdm09-MUT or a mixture of the two at a WT/MUT ratio of 50:50 or 20:80. A slight weight loss of 4 to 6.5% was observed at 2 dpi, but there was no statistically significant difference in body weight among the four groups of ferrets (data not shown). Ferrets had similar temperature profiles and did not show marked differences in other clinical parameters, such as lethargy, sneezing, or interest in food. These observations are similar to those of previous ferret infection studies with H1N1pdm09 (29, 35), as well as studies with A/Brisbane/59/2007-like strains (28, 35) and pre-2007 strains (30). Specific antibodies against H1N1pdm09 were not found in the serum collected before intranasal infection (<10), but all of the ferrets had developed HI antibodies against the virus at 14 dpi.

Nasal washes, collected every 12 h for 72 h and subsequently daily until 7 dpi were analyzed by real-time RT-PCR and viral titration (Fig. 6). Peak viral shedding in all experiments occurred between 48 and 60 h postinfection. Infections with the H1N1pdm09-WT and H1N1pdm09-MUT strains individually (pure populations) were quite similar; e.g., the peak viral RNA and PFU values were identical for the two strains and the decay of virus following the peak was similar (Fig. 6, left). Notably, however, the initial virus increase and the peak value of H1N1pdm09-WT preceded those of H1N1pdm09-MUT by approximately 12 h (the MUT virus population was significantly smaller than that of the WT at 24 and 36 h in terms of both RNA and PFU values; $P = 0.03$ [rank-sum test]). In the 50:50 mixed infections, the H1N1pdm09-WT viral RNA copy number was significantly higher at the peak ($P = 0.03$) and at most other time points. Additionally, the H1N1pdm09-WT virus RNA copy numbers in each mixture were only slightly reduced compared to those in the pure H1N1pdm09-WT infection, while nearly all H1N1pdm09-MUT values were significantly lower than the pure-population infection values. There were no significant differences between the peak nasal wash viral titers (PFU values) in the pure infections and the 80:20 mixture, but the peak titer was significantly lower ($P = 0.05$) for the 50:50 mixture (Fig. 6, bottom row).

DISCUSSION

We performed a set of *in vitro* and ferret infection experiments, with analysis using a mathematical model, to characterize the specific quantitative effects of the H275Y NA mutation on the infection kinetics of the pandemic H1N1 virus (H1N1pdm09) in the absence of treatment with oseltamivir. We found that the H275Y

mutation caused a significant increase in the length of the eclipse phase and a significant reduction in the RNA viral output per MDCKα2,6 cell *in vitro*. The decrease in viral production, however, appears to be compensated for by an increased number of infectious units per MUT virion produced, yielding equivalent infectious-virus production rates, infecting times, and basic reproductive ratios for the two strains. In the analysis of the prior seasonal strain, A/Brisbane/59/2007 (WT and MUT), a similar increase in the eclipse phase length was found for the MUT strain. But in the A/Brisbane/59/2007 background, we found that the H275Y mutation also resulted in a significant decrease in the infecting time and a significant increase in the basic reproductive ratio which could have contributed to the widespread dissemination of the oseltamivir-resistant strain in the population. In mixed infections with equal inocula *in vitro*, the H1N1pdm09-WT strain produced more virus than H1N1pdm09-MUT but likely infected an approximately equal fraction of the cell culture. Infections of ferrets with pure populations of the two virus strains were similar, but mixed infections suggest a replicative advantage for the H1N1pdm09-WT strain.

In general terms, the replication capacity of a particular strain can be considered a balance between the infectivity of the strain (how much virus is produced by infected cells together with how infectious each virion is) and the delay in its growth. In this sense, the longer eclipse period we have found for H1N1pdm09-MUT in MDCKα2,6 cells should be seen as reducing its replicative fitness *in vitro*, since any delay will reduce its ability to infect cells. A shorter infecting time for the MUT strain could potentially yield a compensatory effect, but no significant difference was found for the two H1N1pdm09 strains. The basic reproductive numbers of the two strains were also found to be statistically equivalent. In the analysis of the prior seasonal strain, A/Brisbane/59/2007, we found that the eclipse period was similarly lengthened by the H275Y mutation but that the infecting time of the MUT strain was significantly shorter and its basic reproductive number was significantly larger, suggesting a potentially more advantageous balance between infectivity and delay in that background.

The changes in the infection kinetic parameters which we determined *in vitro* are consistent with the physical changes caused by the H275Y mutation. The conformational change in the NA structure which prohibits efficient bonding with oseltamivir might also impair the function of the NA itself. Reduced affinity for the substrate (i.e., increased K_m) in enzymatic-activity assays is typical for H275Y MUT strains in general (41) and for H1N1pdm09-MUT in particular (9, 12). This impairment would likely cause a delay in the release of progeny virus (a lengthened eclipse phase) and a reduction in the number of virions released from the surface of an infected cell (a reduction in viral production per cell). It is also known that the A/Brisbane/59/2007 strains have increased NA surface expression and activity (6) (relative to H1N1pdm09 and pre-2007 strains), which may lead to generally increased infectivity, consistent with our finding that both the WT and MUT A/Brisbane/59/2007 strains had shorter infecting times than H1N1pdm09-WT. A comprehensive visual analysis—using electron microscopy (29) or fluorescence techniques (33, 44)—of the budding process of H275Y MUTs in comparison with their WT counterparts could shed more light on the mechanism of both the lengthened eclipse period and reduced viral production that we have highlighted here and constitutes an important direction for future work.

The reduction in viral production which is evidently induced by the H275Y mutation allowed H1N1pdm09-WT to dominate the total viral production in competitive-mixture infections *in vitro*. We showed, however, that the observed difference between the total virus amounts produced at a 50:50 infection ratio was consistent with an equal number of cells being infected by each strain (given the higher rate of WT viral production per cell). This suggests that H1N1pdm09-MUT produces a larger proportion of infectious virus than H1N1pdm09-WT. Indeed, we found that the ratio of infectious units to virus particles was 12 times higher for the resistant strain; approximately 60 virions were produced for every successful infection by H1N1pdm09-WT, while only 5 were required per infection for H1N1pdm09-MUT.

In ferrets, experiments suggested a replication advantage for H1N1pdm09-WT over H1N1pdm09-MUT; while the peak viral RNA and PFU loads were identical for infections with either strain alone, the RNA viral load in competitive mixed infections at a 50:50 ratio was dominated by H1N1pdm09-WT. Comparing infections of ferrets with either H1N1pdm09-WT or H1N1pdm09-MUT alone reveals a potential mechanism for this dominance; while the peak RNA and PFU levels of H1N1pdm09-WT and H1N1pdm09-MUT were equal, there was a delay in the growth of H1N1pdm09-MUT virus RNA and PFU levels. Prior experimental infections of ferrets with H1N1pdm09 (12, 15, 31, 45, 46) have not been powered to demonstrate such a difference between the two strains because of less frequent nasal wash sampling and larger initial inocula. A delayed infection by the H1N1pdm09-MUT strain could be related to compromised NA action caused by the mutation (9, 12). While the primary function of NA is to allow the release of progeny virions from a cell surface, a secondary function *in vivo* is to cleave sialic acid in the mucus layer, which aids virus penetration to the respiratory tract epithelium (37). It is important to note in this context that while a certain ratio of WT to MUT virus in the infecting inoculum *in vitro* will result in that ratio of initially infected cells (because the ratio is prepared using titrations on the same culture of cells), this is not necessarily true *in vivo*. An important improvement of the method would allow titration of the inocula on a more relevant cell type, e.g., an *ex vivo* ferret tracheobronchial epithelium.

The strength of our competitive mixed-infection model over the analysis of infections with only pure populations of virus is that it closely mimics natural infections at the crucial moment where strain replacement might occur within a host (see also the recent analysis of A/Brisbane/59/2007 [28]). While previous studies have assessed the replication efficiency of pure populations of H1N1pdm09-WT and H1N1pdm09-MUT *in vitro* and in ferrets (15, 31, 38), most have found similar levels of virus production by the two strains (as we have found), suggesting similar replication capacities. Two recent studies did perform a mixed-infection experiment (12, 45), one of which concluded that the replication capacities were equal (45) while the other found that H1N1pdm09-MUT growth was impaired (12). An important extension of this line of research will be the analysis of mixed-population infections of animals undergoing oseltamivir treatment.

The method we have employed here (analysis of two complementary *in vitro* assays with a mathematical model) enables the extraction of the parameters which characterize viral replication for a given strain. Some of the extracted parameters (viral clearance rate, production rate, and eclipse phase length) can be seen

directly in the experimental viral kinetic time course, providing validation of the method. But the strongest validation is the model's accurate prediction of the kinetics of the competitive mixed-infection experiments *in vitro*. We believe that this new approach to characterizing and quantitatively comparing strains has great potential. For example, it could be applied to characterize the effect of any single mutation by providing a quantitative understanding of the phenotypic differences introduced by the genotypic change. It could also be used to characterize the mode of action of a novel antiviral compound by quantifying the changes it introduces in each phase of viral replication.

ACKNOWLEDGMENTS

This study was supported by a grant from the Canadian Institutes for Health Research (www.cihr-irsc.gc.ca; funding reference numbers 86937 and 111071) (G.B. and C.A.A.B.).

The computational aspects of this work were made possible by the facilities of the Shared Hierarchical Academic Research Computing Network (SHARCNET, www.sharcnet.ca) and Compute/Calcul Canada.

REFERENCES

1. **Abed Y, Goyette N, Boivin G.** 2004. A reverse genetics study of resistance to neuraminidase inhibitors in an influenza A/H1N1 virus. Antivir. Ther. **9**:577–581.
2. **Abed Y, Pizzorno A, Bouhy X, Boivin G.** 2011. Role of permissive neuraminidase mutations in influenza A/Brisbane/59/2007-like (H1N1) viruses. PLoS Pathog. **7**:e1002431. doi:10.1371/journal.ppat.1002431.
3. **Baz M, Abed Y, McDonald J, Boivin G.** 2006. Characterization of multidrug-resistant influenza A/H3N2 viruses shed during 1 year by an immunocompromised child. Clin. Infect. Dis. **43**:1555–1561.
4. **Baz M, et al.** 2009. Emergence of oseltamivir-resistant pandemic H1N1 virus during prophylaxis. N. Engl. J. Med. **361**:2296.
5. **Baz M, Abed Y, Simon P, Hamelin M, Boivin G.** 2010. Effect of the neuraminidase mutation H274Y conferring resistance to oseltamivir on the replicative capacity and virulence of old and recent human influenza A(H1N1) viruses. J. Infect. Dis. **201**:740–745.
6. **Bloom JD, Gong LI, Baltimore D.** 2010. Permissive secondary mutations enable the evolution of influenza oseltamivir resistance. Science **328**: 1272–1275.
7. **Bloom JD, Nayak JS, Baltimore D.** 2011. A computational-experimental approach identifies mutations that enhance surface expression of an oseltamivir-resistant influenza neuraminidase. PLoS One **6**:e22201. doi: 10.1371/journal.pone.0022201.
8. **Bouvier NM, Rahmat S, Pica N.** 2012. Enhanced mammalian transmissibility of seasonal influenza A/H1N1 viruses encoding an oseltamivir-resistant neuraminidase. J. Virol. **86**:7268–7279.
9. **Brookes DW, Miah S, Lackenby A, Hartgroves L, Barclay WS.** 2011. Pandemic H1N1 2009 influenza virus with the H275Y oseltamivir resistance neuraminidase mutation shows a small compromise in enzyme activity and viral fitness. J. Antimicrob. Chemother. **66**:466–470.
10. **Centers for Disease Control and Prevention.** 2009. Update: drug susceptibility of swine-origin influenza A (H1N1) viruses. MMWR Morb. Mortal. Wkly. Rep. **58**:433–435.
11. **Dharan N et al.** 2009. Infections with oseltamivir-resistant influenza A(H1N1) virus in the United States. JAMA **301**:1034–1041.
12. **Duan S, et al.** 2010. Oseltamivir-resistant pandemic H1N1/2009 influenza virus possesses lower transmissibility and fitness in ferrets. PLoS Pathog. **6**:e1001022. doi:10.1371/journal.ppat.1001022.
13. **Efron B, Tibshirani R.** 1986. Bootstrap methods for standard errors, confidence intervals, and other measures of statistical accuracy. Stat. Sci. **1**:77–97.
14. **European Centre for Disease Prevention and Control. August**2011. Bi-weekly influenza surveillance overview 26 August 2011. Technical report, European Centre for Disease Prevention and Control. European Centre for Disease Prevention and Control, Stockholm, Sweden. http://ecdc.europa.eu/en/publications/Publications/110826_SUR_Weekly_Influenza_Surveillance_Overview.pdf.
15. **Hamelin ME, et al.** 2010. Oseltamivir-resistant pandemic A/H1N1 virus is as virulent as its wild-type counterpart in mice and ferrets. PLoS Pathog. **6**:e1001015. doi:10.1371/journal.ppat.1001015.
16. **Hamelin ME, et al.** 2011. Reduced airborne transmission of oseltamivir-resistant pandemic A/H1N1 virus in ferrets. Antivir. Ther. **16**:775–777.
17. **Hatakeyama S, et al.** 2005. Enhanced expression of an α-2,6-linked sialic acid on MDCK cells improves isolation of human influenza viruses and evaluation of their sensitivity to a neuraminidase inhibitor. J. Clin. Microbiol. **43**:4139–4146.
18. **Hauge S, Dudman S, Borgen K, Lackenby A, Hungnes O.** 2009. Oseltamivir-resistant influenza viruses A (H1N1), Norway 2007-2008. Emerg. Infect. Dis. **15**:155–162.
19. **Hayden FG, de Jong M.** 2011. Emerging influenza antiviral resistance threats. J. Infect. Dis. **203**:6–10.
20. **Health Protection Agency.** 20 November 2009, posting date. HPA statement on possible transmission of oseltamivir resistant pandemic influenza A(H1N1). Technical report, Government UK. http://www.hpa.org.uk/webw/HPAweb&HPAwebStandard/HPAweb_C/1258560561316?p=1231252394302.
21. **Herlocher M, et al.** 2004. Influenza viruses resistant to the antiviral drug oseltamivir: transmission studies in ferrets. J. Infect. Dis. **190**:1627–1630.
22. **Holder BP, Beauchemin CA.** 2011. Exploring the effect of biological delays in kinetic models of influenza within a host or cell culture. BMC Public Health **11**:S10. doi:10.1186/1471-2458-11-S1-S10.
23. **Holder BP, Liao LE, Simon P, Boivin G, Beauchemin CA.** 2011. Design considerations in building *in silico* equivalents of common experimental influenza virus assays. Autoimmunity **44**:282–293.
24. **Holder BP, et al.** 2011. Assessing fitness of an oseltamivir-resistant seasonal A/H1N1 influenza strain using a mathematical model. PLoS One **6**:e14767. doi:10.1371/journal.pone.0014767.
25. **Hurt A, et al.** 2012. Characteristics of a widespread community cluster of H275Y oseltamivir-resistant A(H1N1)pdm09 influenza in Australia. J. Infect. Dis. **206**(2):148–157.
26. **Hurt AC, et al.** 2012. Antiviral resistance during the 2009 influenza A H1N1 pandemic: public health, laboratory, and clinical perspectives. Lancet Infect. Dis. **12**:240–248.
27. **Hurt AC, et al.** 2011. Community transmission of oseltamivir-resistant A(H1N1)pdm09 influenza. N. Engl. J. Med. **365**:2541–2542.
28. **Hurt AC, et al.** 2010. Assessing the viral fitness of oseltamivir-resistant influenza viruses in ferrets, using a competitive-mixtures model. J. Virol. **84**:9427–9438.
29. **Itoh Y, et al.** 2009. In vitro and in vivo characterization of new swine-origin H1N1 influenza viruses. Nature **460**:1021–1025.
30. **Ives J, et al.** 2002. The H274Y mutation in the influenza A/H1N1 neuraminidase active site following oseltamivir phosphate treatment leaves virus severely compromised both in vitro and in vivo. Antiviral Res. **55**: 307–317.
31. **Kiso M, et al.** 2010. Characterization of oseltamivir-resistant 2009 H1N1 pandemic influenza A viruses. PLoS Pathog. **6**:e1001079. doi:10.1371/journal.ppat.1001079.
32. **Lackenby A, et al.** 2011. Continued emergence and changing epidemiology of oseltamivir-resistant influenza A(H1N1)2009 virus, United Kingdom, winter 2010-11. Euro Surveill. **16**(5):pii19784. http://www.eurosurveillance.org/ViewArticle.aspx?ArticleId=19784.
33. **Lakadamyali M, Rust MJ, Babcock HP, Zhuang X.** 2003. Visualizing infection of individual influenza viruses. Proc. Natl. Acad. Sci. U. S. A. **100**:9280–9285.
34. **Le QM, et al.** 2010. A community cluster of oseltamivir-resistant cases of 2009 H1N1 influenza. N. Engl. J. Med. **362**:86–87.
35. **Maines TR, et al.** 2009. Transmission and pathogenesis of swine-origin 2009 A(H1N1) influenza viruses in ferrets and mice. Science **325**:484–487.
36. **Marcus PI, Ngunjiri JM, Sekellick MJ.** 2009. Dynamics of biologically active subpopulations of influenza virus: plaque-forming, noninfectious cell-killing, and defective interfering particles. J. Virol. **83**:8122–8130.
37. **Matrosovich MN, Matrosovich T, Gray T, Roberts NA, Klenk HD.** 2004. Neuraminidase is important for the initiation of influenza virus infection in human airway epithelium. J. Virol. **78**:12665–12667.
38. **Memoli MJ, et al.** 2011. Multidrug-resistant 2009 pandemic influenza A(H1N1) viruses maintain fitness and transmissibility in ferrets. J. Infect. Dis. **203**:348–357.
39. **Pizzorno A, Bouhy X, Abed Y, Boivin G.** 2011. Generation and characterization of recombinant pandemic influenza A(H1N1) viruses resistant to neuraminidase inhibitors. J. Infect. Dis. **203**:25–31.

40. **Public Health Agency of Canada.** 2011. Fluwatch 2011, weeks 33 and 34. Technical report, Government of Canada. Public Health Agency of Canada, Ottawa, Ontario, Canada. http://www.phac-aspc.gc.ca/fluwatch/10–11/w34_11/index-eng.php.
41. **Rameix-Welti MA, Enouf V, Cuvelier F, Jeannin P, van der Werf S.** 2008. Enzymatic properties of the neuraminidase of seasonal H1N1 influenza viruses provide insights for the emergence of natural resistance to oseltamivir. PLoS Pathog. **4**:e1000103. doi:10.1371/journal.ppat.1000103.
42. **Renaud C, Kuypers J, Englund JA.** 2011. Emerging oseltamivir resistance in seasonal and pandemic influenza A/H1N1. J. Clin. Virol. **52**:70–78.
43. **Reuman PD, Keely S, Schiff GM, Gamble JN.** 1989. Assessment of signs of influenza illness in the ferret model. J. Virol. Methods **24**:27–34.
44. **Rust MJ, Lakadamyali M, Zhang F, Zhuang X.** 2004. Assembly of endocytic machinery around individual influenza viruses during viral entry. Nat. Struct. Mol. Biol. **11**:567–573.
45. **Seibert CW, et al.** 2010. Oseltamivir-resistant variants of the 2009 pandemic H1N1 influenza A virus are not attenuated in the guinea pig and ferret transmission models. J. Virol. **84**:11219–11226.
46. **Seibert CW, Rahmat S, Krammer F, Palese P, Bouvier NM.** 2012. Efficient transmission of pandemic H1N1 influenza viruses with high-level oseltamivir resistance. J. Virol. **86**:5386–5389.
47. **Storms A, et al.** 2012. Oseltamivir-resistant pandemic (H1N1) 2009 virus infections, United States, 2010-11. Emerg. Infect. Dis. **18**:308–311.
48. **van der Vries E, et al.** 2010. Evaluation of a rapid molecular algorithm for detection of pandemic influenza A (H1N1) 2009 virus and screening for a key oseltamivir resistance (H275Y) substitution in neuraminidase. J. Clin. Virol. **47**:34–37.

Supplemental Information:
Holder and Pinilla, et. al. Submission to Journal of Virology

December 31, 2011

Analysis of the A/Brisbane/59/2007 (H1N1) seasonal influenza strain from 2007-2009, presented in the manuscript (Table 2), is identical to that performed on H1N1pdm09, with the omission of RNA copy data for the MC experiment. This data was obtained and presented previously [1]. Best fits of the model to the data and histograms of the bootstrap-replicate–derived parameter values are given in Figure 1.

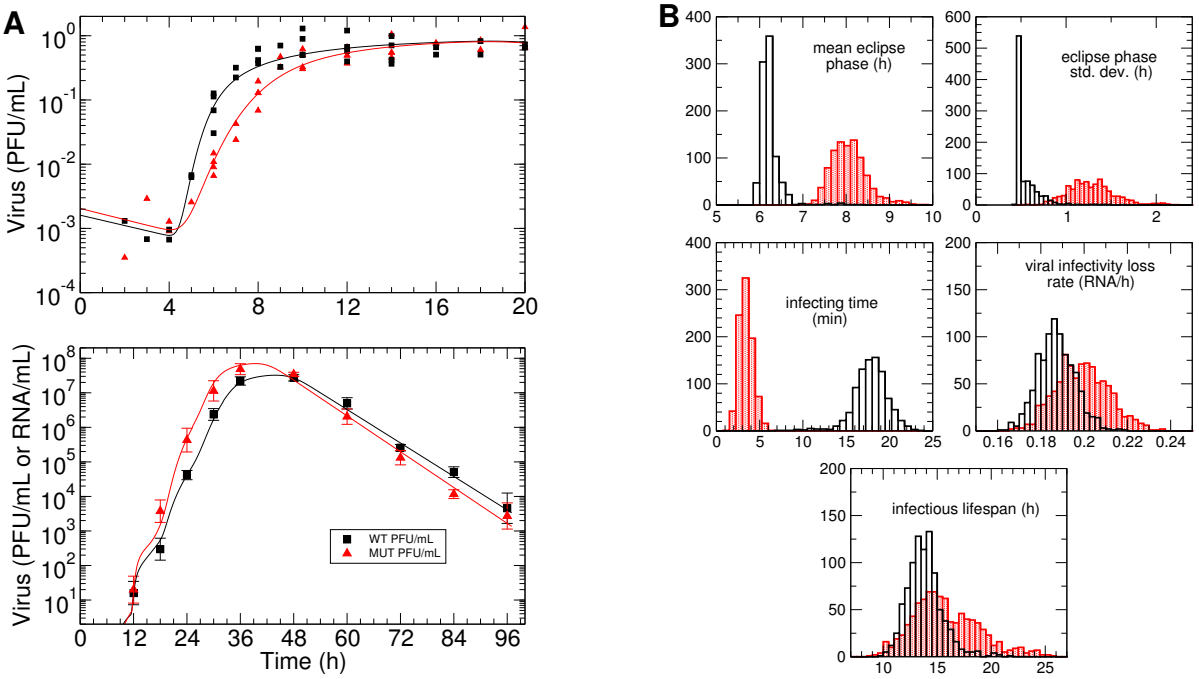

Figure 1: **Single-cycle and multiple-cycle viral yield experiments and fits for A/Brisbane/59/2007 (H1N1).** **A** Experimental viral titer for A/Brisbane/59/2007 WT (squares, black) and MUT (triangles, red) strains in the single-cycle (top left) and multiple-cycle (bottom left) viral yield experiments. Best fit model virus curves are over-plotted as lines. **B** Histograms of parameter values (right) determined from fits to 1000 bootstrap replicates of the MC and SC data for the A/Brisbane/59/2007 WT (black) and MUT (red).

References

[1] **Holder BP, Simon P, Liao LE, Abed Y, Bouhy X, Beauchemin CA, and Boivin G**, 2011. Assessing fitness of an oseltamivir-resistant seasonal A/H1N1 influenza strain using a mathematical model. PLoS One **6**:e14767. doi:10.1371/journal.pone.0014767.